Supplementary information

Dual-molten-salt engineering of accessible active sites in single-atom Fe-NC catalysts

Peng Yu,[a] Yazhou Zhou,[a,b] Guangbo Chen,[*c] Xiafang Tao[*b,d]

[a]School of Materials Science and Engineering, Jiangsu University, Zhenjiang 212013, China.

[b]Nanotechnology Centre, Centre for Energy and Environmental Technologies (CEET), VŠB-Technical University of Ostrava, 17. listopadu 2172/15, Ostrava-Poruba 708 00, Czech Republic

[c]Key Laboratory of Photochemical Conversion and Optoelectronic Materials, Technical Institute of Physics and Chemistry, Chinese Academy of Sciences, Beijing, 100190 China.

[d]Max Planck Institute for Polymer Research, 55128 Mainz, Germany

This file includes:

1. Methods

Preparation of ZIF-8. 3.58 g of $Zn(NO_3)_2 \cdot 6H_2O$ was dissolved in 300 mL of methanol. 3.94 g of 2-methylimidazole was dissolved in 300 mL of methanol. The two solutions were then mixed and maintained at 60 °C under continuous stirring for 24 h. The resulting precipitate was collected by centrifugation, washed three times with methanol, and dried under vacuum to obtain ZIF-8 powder.

Preparation of NC Support. NC supports were prepared via a molten-salt-assisted pyrolysis of ZIF-8. Typically, ZIF-8 was physically mixed with NaCl and KCl by gentle grinding with a mortar and pestle for 10 min. The mixture was pyrolyzed at 910 °C for 2 h under an Ar atmosphere with a heating rate of 5 °C min^{-1}, followed by natural cooling to room temperature. The product was washed three times with deionized water to remove any residual NaCl, then dried at 80 °C overnight. The typical mass ratio of ZIF-8: NaCl: KCl was 1:0.25:0.75, and the resulting sample was denoted as NC/NaK. For comparison, NC/NaCl and NC/KCl were prepared using ZIF-8: NaCl = 1:1 and ZIF-8: KCl = 1:1, respectively, while salt-free NC was obtained by direct pyrolysis of ZIF-8 under identical conditions.

Preparation of Fe-NC catalysts. Fe-NC catalysts were prepared via an impregnation-pyrolysis method. Typically, 50 mg of NC supports (NC, NC/NaCl, NC/KCl, or NC/NaK) were dispersed in 50 mL of methanol by ultrasonication. 5 mg of iron ethylenediaminetetraacetic acid sodium salt (Fe-EDTA) was dissolved in methanol and then added to the above suspension. The mixture was stirred for 12 h to ensure sufficient adsorption of the Fe precursor onto the carbon supports. The resulting solid was collected by centrifugation, washed with methanol, and dried under vacuum at 60 °C. Subsequently, the dried powder was subjected to a second pyrolysis at 900 °C for 1 h under an Ar atmosphere with a heating rate of 10 °C min^{-1}, followed by natural cooling to room temperature. The obtained catalysts were denoted as Fe-NC, Fe-NC/NaCl, Fe-NC/KCl, and Fe-NC/NaK, respectively.

2. Characterizations

The morphology and microstructure of the samples were characterized by transmission electron microscopy (TEM, JEM-1400plus) and high-resolution TEM (HRTEM, JEOL JEM-2100F). Aberration-corrected high-angle annular dark-field scanning TEM (AC-HAADF-STEM, FEI Themis Z) was employed to examine the dispersion of Fe species. X-ray diffraction (XRD, Bruker D8 Advance, Cu Kα radiation, λ = 1.54 Å) was used to analyze the crystal structure. The specific surface area and pore size distribution were determined by N_2 adsorption–desorption measurements (Quantachrome Autosorb IQ MP) using the Brunauer–Emmett–Teller (BET) and density functional theory (DFT) methods. The elemental composition and chemical states were analyzed by X-ray photoelectron spectroscopy (XPS, Thermo Scientific K-Alpha). The Fe loading was quantified by inductively coupled plasma optical emission spectroscopy (ICP-OES, Agilent 5110). X-ray absorption fine structure (XAFS) measurements at the Fe K-edge were performed at the 1W1B beamline of the Shanghai Synchrotron Radiation Facility (SSRF), operated at 2.5 GeV with a maximum current of 250 mA. The extended X-ray absorption fine structure (EXAFS) data were processed and analyzed using the ATHENA

module implemented in the IFEFFIT software package according to standard procedures.

3. Electrochemical Measurements

Electrochemical measurements were carried out on a CHI760E electrochemical workstation using a standard three-electrode configuration at room temperature. A rotating disk electrode (RDE) or rotating ring-disk electrode (RRDE, glassy carbon, 5 mm diameter) was used as the working electrode, with a carbon rod as the counter electrode and an Ag/AgCl (3 M KCl) electrode as the reference electrode. The catalyst ink was prepared by dispersing 2.5 mg of catalyst in a mixed solution of 490 μL ethanol and 10 μL Nafion solution (5 wt%) under ultrasonication. Then, 30 μL of the ink was drop-cast onto the glassy carbon electrode, resulting in a catalyst loading of ~0.76 mg cm^{-2}. Cyclic voltammetry (CV) was conducted in N_2- and O_2-saturated 0.5 M H_2SO_4 at a scan rate of 50 mV s^{-1}. Linear sweep voltammetry (LSV) was performed in O_2-saturated 0.5 M H_2SO_4 at a scan rate of 5 mV s^{-1} with a rotation speed of 900 rpm. RRDE measurements were conducted with the ring electrode held at 1.2 V (vs. RHE) to determine the H_2O_2 yield and electron transfer number. For comparison, Pt/C catalyst was tested in 0.1 M $HClO_4$ to avoid performance loss caused by bisulfate adsorption. All potentials were converted to the reversible hydrogen electrode (RHE) scale. according to the following equation.

$$E(RHE) = 0.059pH + E(Ag/AgCl) + E_0(Ag/AgCl) \quad (1)$$

The yield of hydrogen peroxide and the number of electron transfers are calculated by the following equations:

$$H_2O_2(\%) = 200 \times \frac{I_r/N}{I_d + I_r/N} \times 100\%$$

$$n = 4 \times \frac{I_d}{I_d + I_r/N} \quad (2)$$

*I*r is the ring current, id is the disk current, and N = 0.37 is the Pt ring current.

4. Quantification of the Active Sites

The density of Fe active sites of Fe-NC materials were determined according to the method described by Malko et al (doi.org/10.1038/ncomms13285, Nat. Commun. 7, 13285 (2016). The calculation formula is as follows:

$$SD\left(site\ g^{-1}\right) = \frac{Q_{strip} \times N_A}{n_{strip} \times F \times m_{cat}}$$

(4)

$$TOF\left(e^{-}\cdot site^{-1}\cdot s^{-1}\right) = \frac{i_k \times N_A}{SD \times nF}$$

(5)

where Q_{strip} (C g^{-1}) refers to the excess Coulomb charge associated with the stripping peak, F refers to Faraday's constant (F = 96485 C mol^{-1}), N_A Avogadro's constant (N_A=6.02× 10^{23}), n_{strip} refers to the number of electrons associated with the reduction of one nitrite per site (n_{strip}= 5), L_{cat} refers to the mass of the catalyst, and J_k refers to the kinetic current density ($i_k = \frac{i_L \times i}{i_L - i}$), i (A g^{-1}) is the current and i_L is the limit diffusion current at 0.8 V (RHE) in the LSV curve. Loading of Fe-NC was 0.76 mg cm^{-2}.

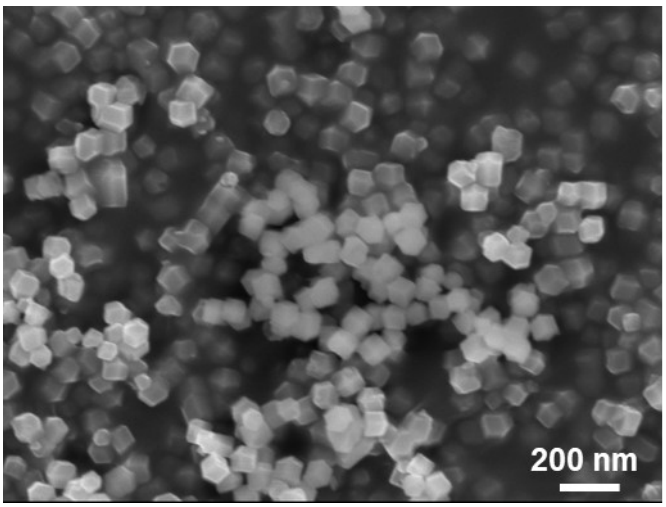

Fig. S1 SEM images of ZIF-8.

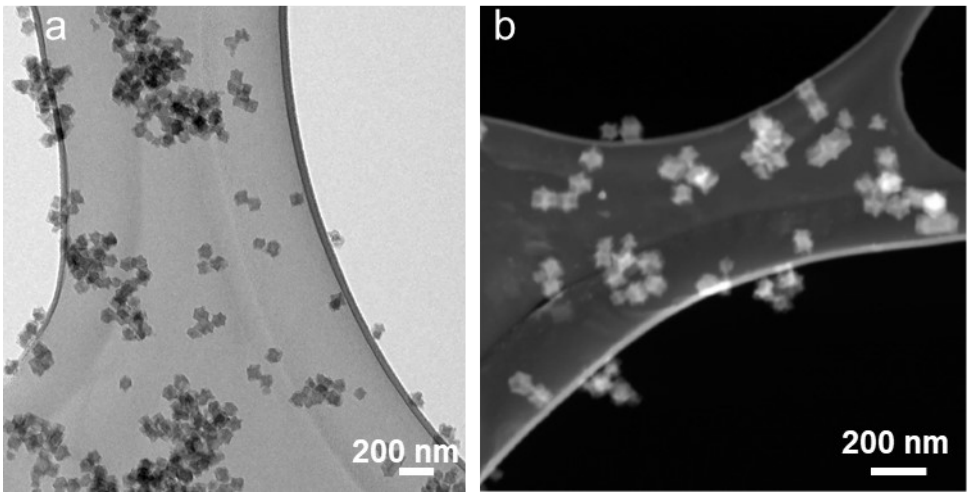

Fig. S2 (a) TEM and (b) HAADF-STEM images of salt-free NC.

Table S1. Porosity properties of the NC supports.

Catalyst	**BET surface area ($m^2 g^{-1}$)**	**Micropore area ($m^2 g^{-1}$)**	**External surface area ($m^2 g^{-1}$)**
NC	1341.4	1046.7	294.8
NC/NaCl	1724.8	1367.7	357.1
NC/KCl	2590.1	1988.0	602.1
NC/NaK	2243.5	1841.1	402.5

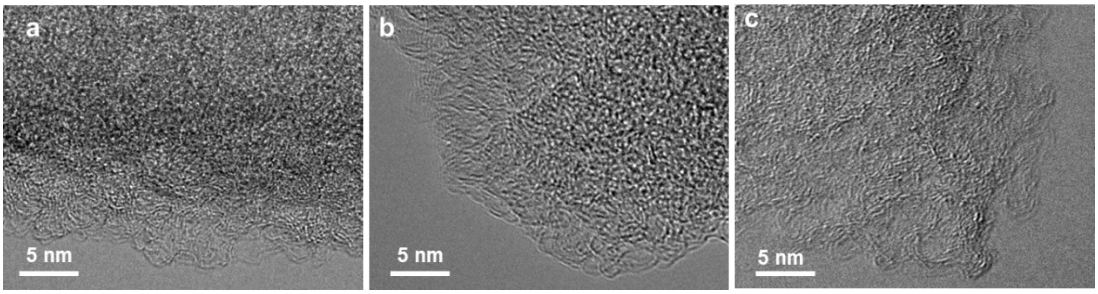

Fig. S3 High-resolution TEM images of (a) Fe-NC, (b) Fe-NC/NaCl, and (c) Fe-NC/KCl.

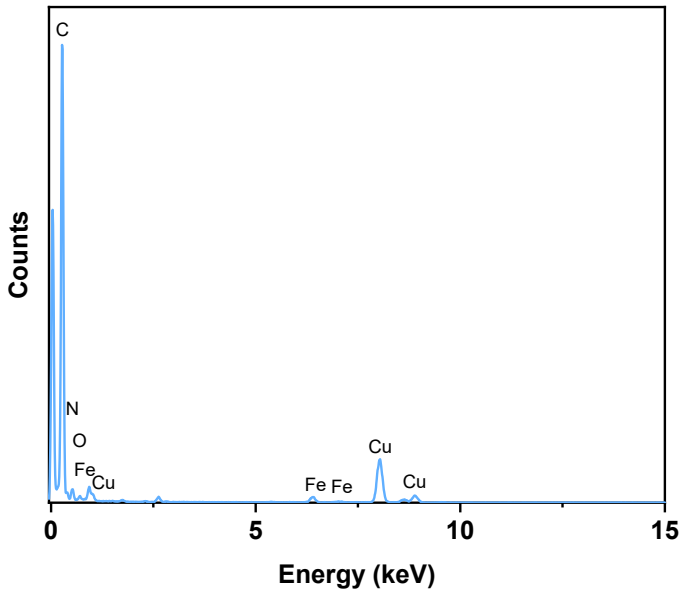

Fig. S4. TEM-EDS spectrum of Fe-NC/NaK.

Table S2. Fe loadings in Fe-NC materials by ICP-OES tests.

Catalyst	Fe loading (wt%)
Fe-NC	1.1
Fe-NC/NaCl	1.3
Fe-NC/KCl	1.4
Fe-NC/NaK	1.4

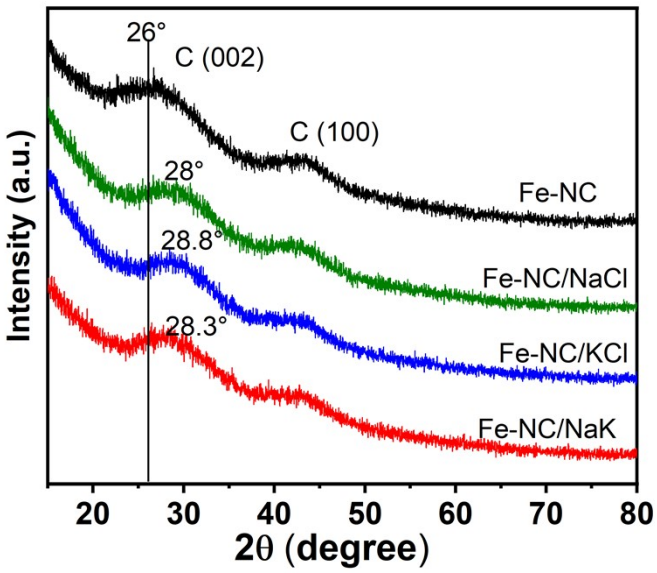

Fig. S5 XRD patterns of Fe-NC, Fe-NC, Fe-NC/NaCl, Fe-NC/KCl, and Fe-NC/NaK.

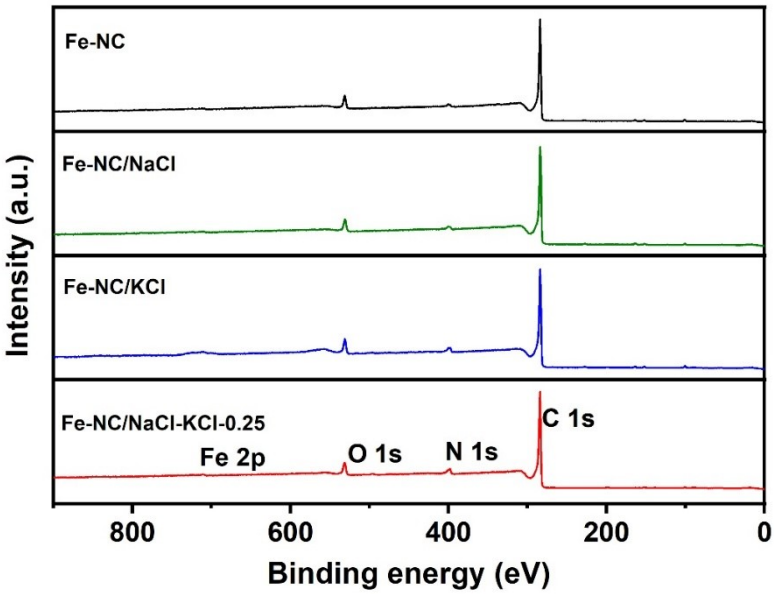

Fig. S6 XPS survey spectra of Fe-NC/NaK, Fe-NC/NaCl, Fe-NC/KCl, and Fe-NC

Table S3. Fitting results for C 1s spectra of the Fe-NC/NaK, Fe-NC/KCl, Fe-NC/NaCl, and Fe-NC.

.

Catalyst	**C=C**	**C-N/C-O**	**C=0**	**π-π**
Binding energy	284.8 (eV)	286 (eV)	288.5 (eV)	290.5(eV)
Fe-NC/NaK	57.6	23.14	8.39	10.83
Fe-NC/KCl	60.31	18.56	12.69	8.43
Fe-NC/NaCl	60.69	14.79	10.45	14.06
Fe-NC	65.18	14.69	11.36	8.78

Table S4. Fitting results for N 1s spectra of the Fe-NC/NaK, Fe-NC/KCl, Fe-NC/NaCl, and Fe-NC.

Catalyst	Pyridinic N (%)	Pyrrolic N (%)	Graphitic N (%)	Fe-N (%)	Oxidized N (%)
Binding energy	398.5 (eV)	400.8 (eV)	401.5 (eV)	399.7 (eV)	403.4 (eV)
Fe-NC/NaK	43.0	14.6	13.7	14.2	14.4
Fe-NC/KCl	38.8	15.7	11.5	15.3	18.4
Fe-NC/NaCl	29.1	16.8	22.2	17.2	14.5
Fe-NC	28.6	21.8	21.6	8.8	19.1

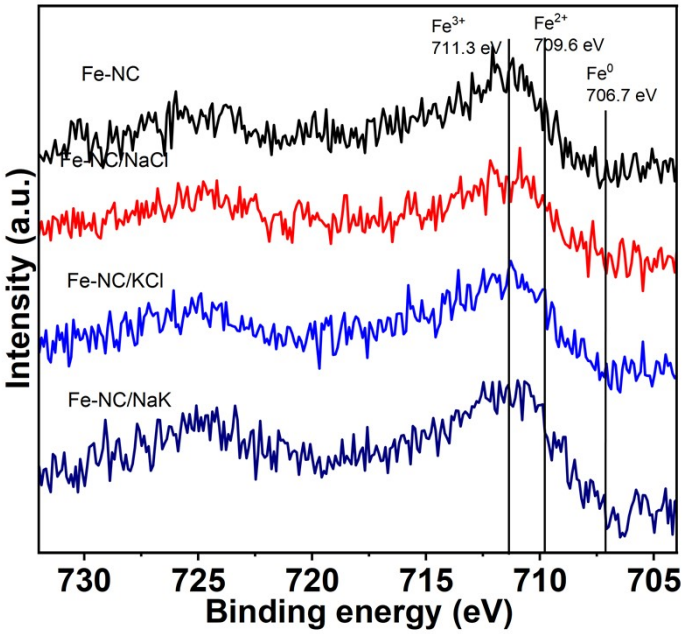

Fig. S7 High-resolution Fe 2p XPS spectra for Fe-NC/NaK, Fe-NC/NaCl, Fe-NC/KCl, and Fe-NC.

Table S5. Structural parameters of the Fe-NC/NaK extracted from the EXAFS fitting. The FeO, Fe_2O_3, and Fe foil were reference materials.

Sample	Path	*N*	*R* (Å)	σ^2 ($\times 10^{-3}$ Å^2)	ΔE_0 (eV)	*R*, %
Fe foil[a]	Fe-Fe	**8**	2.47±0.01	5±1	6±2	0.53
	Fe-Fe	**6**	2.85±0.01	6±2		
FeO	Fe-O	6	2.12 ± 0.02	14.9 ± 2.1	-1.53 ± 0.5	0.009
	Fe-Fe	12	3.06 ±0.01	11.74±1.0	-2.61±1.1	
Fe_2O_3	Fe-O	6	1.96 ± 0.03	10.95 ± 2.1	7.51± 3.2	0.018
	Fe-Fe	6	2.98±0.02	8.85±1.72		
Fe-NC/NaK[b]	Fe-N/O	6.0±0.6	2.00±0.02	11±1	-6±1	0.42

[a]: *k* range: 3-13.6 (Å^{-1}); *R* range: 1-3 Å;[f]: *k* range: 3-12 (Å^{-1}); *R* range: 1.0-2 Å; $S_0^2 = 0.68$ and determined from Fe foil. The bolded numbers represent fixed coordination numbers

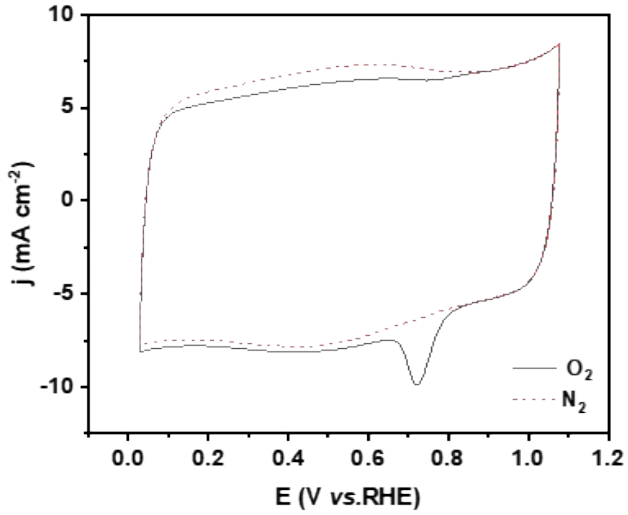

Fig. S8 CV curves of Fe-NC/NaK at a scan rate of 5 mV s^{-1} in O_2/N_2-saturated 0.5 M H_2SO_4.

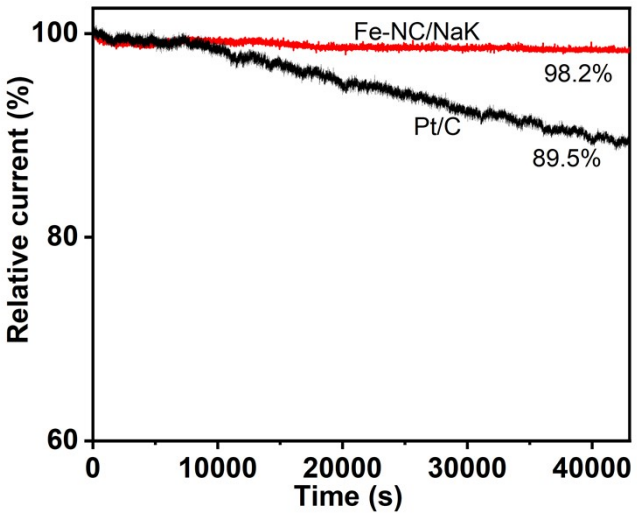

Fig. S9 Chronoamperometric stability of Fe-NC/NaK and Pt/C measured at 0.82 V (vs. RHE) in O_2-saturated 0.5 M H_2SO_4.

Table S6. ORR performance parameters of Fe-NC samples and Pt/C.

Catalyst	E_{onset} (V)	$E_{1/2}$ (V)	J_L (mA cm^{-2})	J_k@0.80 V (mA cm^{-2})	Tafel slope (mV dec^{-1})
Fe-NC	0.87	0.77	-4.2	1.4	66
Fe-NC/NaCl	0.88	0.79	-3.9	2.7	64
Fe-NC/KCl	0.89	0.80	-3.8	3.5	63
Fe-NC/NaK	0.91	0.82	-4.0	9.7	55
Pt/C	0.94	0.83	-4.5	13.1	50

Table S7. Summary of Fe loading, SD, utilization, and TOF of Fe sites for Fe-NC catalysts, derived from nitrite stripping and kinetic current analysis.

Catalyst	Fe loading (wt%)	SD (sites g^{-1})	Utilization (%)	TOF (e^-·site^{-1} s^{-1})
Fe-NC	1.1	9.1×10^{18}	7.7	1.2
Fe-NC/NaCl	1.3	1.4×10^{19}	10	1.6
Fe-NC/KCl	1.4	2.3×10^{19}	15.2	1.2
Fe-NC/NaK	1.4	4.0×10^{19}	27	2.0

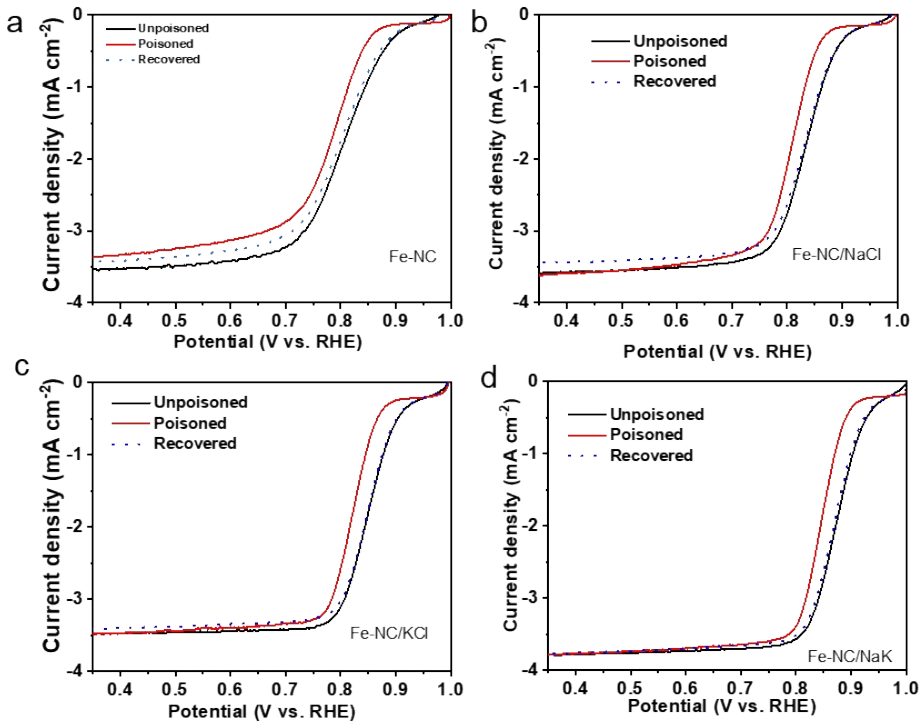

Fig. S10 Determination of the site density (SD) of Fe site. ORR LSV curves before, during and after nitrite adsorption in an O_2-saturated 0.5 M acetate buffer at pH 5.2 for (a) Fe-NC, (b) Fe-NC /NaCl, (c) Fe-NC /KCl, and (d) Fe-NC /NaK. Catalyst loading: 0.27 mg cm^{-2}.

Table S8. Comparison of structural and electrochemical properties of Fe-N-C catalysts reported in the literature. SD: site density, Utilization of active sites. Some parameters were not reported in the original papers and are indicated as "—".

Catalyst	**BET area(m^2 g^{-1})**	**SD ($\times10^{19}$sites g^{-1})**	**Utilization (%)**	$E_{1/2}$	**Ref**
Fe-NC/NaK	**2243**	**4**	**27**	**0.82(H_2SO_4)**	**This work**
Fe-N/C	1145	1.42	1.85	—	[1]
Fe-N-C-SMV	1048.6	2.48	17.69	0.84(H_2SO_4)	[2]
MC-Fe-NC	1068	5.62	—	0.81(H_2SO_4)	[3]
TPI@Z8(SiO_2) 650-C	1648	3.42	11.4	—	[4]
nano-e-FeNC	—	2.41	—	0.83(H_2SO_4)	[5]
3D Fe-N-C	1399.15	3.16	21.9	0.82(H_2SO_4)	[6]
Fe-pyridinic N-C	1371	—	—	0.82($HClO_4$)	[7]
Fe@ Fe-N-C	1290	—	—	0.82($HClO_4$)	[8]
CNRS	840	1.44	2.5	—	[9]
Fe_{SA}/Fe_{AC}-2DNPC	995.4	2.01	—	0.81(H_2SO_4)	[10]
Fe-N-C_{NH4I}	1413.7	2.15	10.3	0.924(KOH)	[11]
Fe-SA/N-HCS	1682.3	11	21	0.91(KOH)	[12]
FeNC-CVD-750	—	19.2	100	0.85(H_2SO_4)	[13]

Supporting References

1. M. Gong, A. Mehmood, B. Ali, K. W. Nam and A. Kucernak, *ACS Catal.*, 2023, 13, 6661-6674.
2. J. Li, C. Lin, Z. Chen, J. Huang, B. Yang, M. Lin, P. K. Shen and Z. Q. Tian, *ACS Catal.*, 2025, 15, 20512-20530.
3. Y. Guan, L. Gao, D. Wu, J. He, H. Luo, Q. Liu, Y. Zhou, J. Luo, R. Li, Z. Kang, J. Li, X. Tian, S. Chen and Z. Miao, *J. Energy Chem.*, 2026, https://doi.org/10.1016/j.jechem.2026.04.050
4. X. Wan, X. Liu, Y. Li, R. Yu, L. Zheng, W. Yan, H. Wang, M. Xu and J. Shui, *Nat. Catal*., 2019, 2, 259-268.
5. Q. Liu, W. Liu, X. Wan, W. Chen, X. Liu, X. Liu, J. Shang, J. Miao, D. Su, X. Sun and J. Shui, *Adv. Funct. Mate*r., 2025, 35, 2507376.
6. R. Wang, Y. Yang, Y. Zhao, L. Yang, P. Yin, J. Mao and T. Ling, *J. Energy Chem.*, 2021, 58, 629-635.
7. L. Li, Y. Wen, G. Han, Y. Liu, Y. Song, W. Zhang, J. Sun, L. Du, F. Kong, Y. Ma, Y. Gao, J. Wang, C. Du and G. Yin, *Chem. Eng. J*., 2022, 437, 135320
8. L. Li, Y. Wen, G. Han, F. Kong, L. Du, Y. Ma, P. Zuo, C. Du and G. Yin, *Small*, 2023, 19, 2300758.
9. M. Primbs, Y. Sun, A. Roy, D. Malko, A. Mehmood, M.-T. Sougrati, P.-Y. Blanchard, G. Granozzi, T. Kosmala, G. Daniel, P. Atanassov, J. Sharman, C. Durante, A. Kucernak, D. Jones, F. Jaouen and P. Strasser, *Energy Environ. Sci*., 2020, 13, 2480-2500.
10. X. Wan, Q. Liu, J. Liu, S. Liu, X. Liu, L. Zheng, J. Shang, R. Yu and J. Shui, *Nat. Commun*, 2022, 13, 2963.
11. J. Liu, Y. Liu, B. Nan, D. Wang, C. Allen, Z. Gong, G. He, K. Fu, G. Ye and H. Fei, *Angew. Chem. Int. Ed. Engl*., 2025, 64, e202425196.
12. L. Zong, K. Fan, L. Cui, F. Lu, P. Liu, B. Li, S. Feng and L. Wang, *Angew. Chem. Int. Ed. Engl*., 2023, 62, e202309784.
13. L. Jiao, J. Li, L. L. Richard, Q. Sun, T. Stracensky, E. Liu, M. T. Sougrati, Z. Zhao, F. Yang, S. Zhong, H. Xu, S. Mukerjee, Y. Huang, D. A. Cullen, J. H. Park, M. Ferrandon, D. J. Myers, F. Jaouen and Q. Jia, *Nat. Mater*, 2021, 20, 1385-1391.